Advanced Ceramics Progress: Vol. 7, No. 4, (Autumn 2021) 10-19

Materials and Energy Research Center
MERC

Contents lists available at ACERP

Advanced Ceramics Progress

Journal Homepage: www.acerp.ir

Original Research Article

Fabrication and Preliminary Characterization of Tissue Engineering Scaffolds Based on Alumina/Bioactive Glass

S. Borhan [a,*], M. R. Badr-Mohammadi [b], S. Hesaraki [c], J. Esmaeilzadeh [d]

[a] *Assistant Professor, Department of Materials, Chemical and Polymer Engineering, Imam Khomeini International University-Buin Zahra Higher Education Center of Engineering and Technology, Buin Zahra, Qazvin, Iran*

[b] *MSc, Department of Nanotechnology and Advanced Materials, Materials and Energy Research Center (MERC), Meshkindasht, Alborz, Iran*

[c] *Professor, Department of Nanotechnology and Advanced Materials, Materials and Energy Research Center (MERC), Meshkindasht, Alborz, Iran*

[d] *Assistant Professor, Department of Materials and Chemical Engineering, Esfarayen University of Technology, Esfarayen, North Khorasan, Iran*

* Corresponding Author Email: shkfborhan@bzte.ac.ir (S. Borhan)

URL: https://www.acerp.ir/article_143925.html

ARTICLE INFO

Article History:

Received 06 January 2022
Received in revised form 26 January 2022
Accepted 29 January 2022

Keywords:

Alumina Scaffold
Bioactive Glass
Cell Culture
Coating
Porosity

ABSTRACT

Many researches have been conducted so far to improve the bioactivity and mechanical properties of bioceramic-based scaffolds in order to stimulate tissue attachment to the implant surface and create a stable bonding. In this research, Al_2O_3 scaffolds were prepared using different types of polyurethane foam through template replica method and then, they were sintered at 1650 °C. A sol of SiO_2–CaO– P_2O_5–MgO system Bioactive Glass (BG) was synthesized where the scaffolds were soaked and heat-treated at 800 °C based on thermo gravimetry analysis. X-ray diffraction confirmed the presence of silica in the structure of BG coating diffused in alumina scaffold that caused the formation of sillimanite phase. According to Scanning Electron Microscopy (SEM) analysis, all prepared scaffolds were highly porous, and the mean porosity percentage was approximately 85 %. The compressive strength and porosity percentage of the scaffolds nearly ranged between 0.35-1.75 MPa and 79-93 %, respectively. The sample with the best result of compressive strength was considered as the optimum alumina scaffold (OAS). In vitro acellular behavior of the samples was also evaluated followed by soaking them in the simulated body fluid, and the ball-like morphology including entangled needle-like crystals were observed on the surface of the sample. Moreover, cells were cultured in alumina scaffolds with and without BG coating and in the cell studies. According to the findings, both samples supported attachment and proliferation of osteoblasts. Therefore, Based on the scaffold porosity percentage which promotes cell attachment as well as the compressive strength which is close to that of the trabecular bone, it can be concluded that application of BG-coated alumina scaffold as a bone-healing material may be beneficial.

https://doi.org/10.30501/ACP.2022.323414.1079

1. INTRODUCTION

Bone tissue injuries significantly affect the lives of millions of people worldwide. Some common treatment methods such as autologous and allogeneic bone grafting cannot produce the ideal therapeutic effect; to be specific, allograft bone transplantation may cause sevral side effects such as negligible osseointegration, immune rejection, and blood disease. To overcome these problems, Bone Tissue Engineering (BTE) was

Please cite this article as: Borhan, S., Badr-Mohammadi, M. R., Hesaraki, S., Esmaeilzadeh, J., "Fabrication and Preliminary Characterization of Tissue Engineering Scaffolds Based on Alumina/Bioactive Glass", ***Advanced Ceramics Progress***, Vol. 7, No. 4, (2021), 10-19. https://doi.org/10.30501/ACP.2022.323414.1079

introduced to promote the already available techniques for lost bone regeneration using a combination of cells, growth factors, and biomaterials, maintain the stable state of tissue, and enhance/replace the function of target tissues. This approach enjoys several advantages such as high flexibility, low risk of infection, and great biocompatibility [1-3].

Tissue Engineering (TE) is currently used as a considerable successful technique in a wide variety of fields to repair and reconstruct tissues and organs such as bone, skin, cartilage, liver, bladder, ligament, nerves, cardiac valves, etc. This is the main reason why TE is still an interesting subject of many investigations. The overall objective of TE scaffolds is to provide the cells with a temporary matrice to generate new tissues of favorable shapes and dimensions. Of note, given that the scaffold should be characterized by suitable physical, mechanical, and biological properties, one of the challanges in TE is construction of a porous biodegradable scaffold. Moreover, it should possess individual and particular morphology and microstructure [4,5].

A number of different scaffolds (organic and inorganic or hybrid of them) have been fabricated so far among which, bioceramic scaffolds are amazingly appreciated owing to their unique properties such as biocompatibility and biodegradability. However, along with these appropriate characteristics, they also have some mechanical properties. In this regard, many studies have been conducted to overcome this weakness [6,7].

Alumina scaffolds are extensively used owing to their high biocompatibility, excellent wear resistance, and hardness; however, they are inert in body. Therefore, the combination of Alumina scaffolds with a bioactive material would result in a better biocompatibility and maintenance. Kim et al. evaluated Tricalcium Phosphate (TCP) coated and non-coated alumina scaffolds. TCP-coated scaffols exhibit favorable bone tissue ingrowth [8]. Naga et al. condusted a study on the bioactivity of the porous alumina scaffolds coated with calcium pyrophosphate. Histological analysis revealed that the produced scaffold can be used as the bone substitute [9]. In another research, porous alumina matrice was dipped into bioglass/hydroxyapatite ceramic slurry and then sintered. The evaluation confirmed the higher cell interaction of the coated porous alumina than that of non-coated alumina scaffolds [10].

The main objective of the current research is to prepare an alumina scaffold to obtain good mechanical properties and coat it by a ternary system of bioactive glass (BG) to obtain suitable bioactivity. Alumina is a bioinert ceramic with fantastic mechanical strength, yet it is not bioactive [11]. In contrast to alumina, BG is a kind of bioceramic with the ability to bond with host tissues through formation of a calcium phosphate layer at their interface to live tissues. However, it has a considerable drawback, i.e., low mechanical strength [12]. It seems that the alumina coated with BG produces a bioactive scaffold with proper mechanical properties.

2. MATERIALS AND METHODS

2.1. Preparation of Specimens

Alumina scaffolds were made using polyurethane foams. First, alumina (Martoxid® MR70, Albemarle, Germany), distilled water, and polyvinyl alcohol (PVA, 363138 Aldrich, Germany), as the binder, were mixed together and milled for 24 h to achieve a homogenous slurry. Then, the foam samples of 1×1×1 cm^3 in dimention were immersed in the slurry of alumina to smear all sides of the foams. Next, the foams were taken out from the suspension and squeezed to remove the excessive slurry. In this step, three types of polyurethane were used (30, 45, and 60 Pores Per Inch (PPI)). The foams were then dried at 70 °C and sintered with a certain heat-treatment program. Samples were then heated to 300 °C with the rate of 1 °C/min and remained at 300 °C for one hour to remove polymeric substrate. Finally, they were heated to 1650 °C at a rate of 5 °C/min and then sintered and stabilized at this temperature for three hours [11].

BG based on 64 SiO_2, 26 CaO, 5 MgO, and 5 P_2O_5 (% mol) system was synthesized based on water-based sol-gel process. In this process, 13.33 g of Tetraethyl Orthosilicate (TEOS, 800625 Merck, Germany) was poured into 30 mL of 0.1 M Nitric Acid (HNO_3, 1004562500 Merck, Germany) solution and stirred for one hour at room temperature to complete acid hydrolysis. The following compounds were added in sequence, giving 45 min to each reagent to react completely: 0.91 g triethylphosphate (TEP: 821141 Merck, Germany), 6.14 g of calcium nitrate tetrahydrate ($CaNO_3.4H_2O$, 102123 Merck, Germany), and 1.28 g of magnesium nitrate hexahydrate ($Mg(NO_3)_2$, Merck 107871, Germany). After the final addition, the mixture was stirred for an hour to obtain a transparent sol. Now, it is ready to be used for coating on alumina scaffolds.

In this stage, the sintered scaffolds were soaked in the BG sol for a few seconds. This procedure was repeated three times to obtain appropriate coatings. At the end, the coated samples were dried at 70 °C for 24 h. The sintering temperature was 800 °C in accordance with the Thermo-Gravimetric Analysis (TGA) of BG. The resultant scaffolds were heat-treated at this temperature for two hours to obtain the proper chemical bonding between the glass and alumina.

2.2. TGA and DTA Analyses

The thermal behavior of BG was studied through Differential Thermal Analysis (DTA) and Thermo Gravimetry (TG) analysis. For this purpose, the obtained sol was poured into a cylindrical teflon container and kept sealed for 10 days at room temperature until the

occurance of the polycondensation reaction. The formed gel was dried at 70 °C for 3 days and then at 120 °C for 2 days. The dried gel was analyzed using PL-STA 1600-England apparatus under the air atmosphere and heated from room temperature to 1200 °C with the heating rate of 10 °C/min.

2.3. X-Ray Diffraction Analysis

Phase analysis of the scaffolds was carried out using a Philips PW3710 diffractometer. This apparatus worked with the voltage of 40 kV, current of 30 mA, and applied Cu-Kα radiation (1.54 Å). The required data were collected in the range of $10° \leq 2\theta \leq 80°$ at the scan speed of 2 °/min.

2.4. Morphology Observations

The morphologies of the pores and pore walls in the scaffolds were observed using Scanning Electron Microscopy (SEM) (Stereoscan S360-Cambridge, UK), fucnctioning at the acceleration voltage of 15 kV. First, samples were coated with a thin layer of Au using the sputtering instrument. The elemental image analysis of the scaffolds was determined by Energy Dispersive Spectroscopy (EDS) that was directly connected to SEM. According to previous similar studies [13-15], the pore size was measured by Image J software, and the mean porosity diameter was defined as the pore size of scaffolds.

2.5. Porosity Percentage Measurement of Scaffolds

To measure the porosity percentage of the scaffolds, they were well-milled by agate mortar. The true density of the sintered powder was calculated based on the standard ASTM D 2320-87 through pycnometer method. The amounts of mass and volume were also calculated to measure the bulk density of the sintered samples.

2.6. Mechanical Test

The mechanical properties of the samples were measured based on compressive strength test. The cylindrical samples were fabricated (15 mm in diameter and 20 mm in height), and the compressive strength of the samples was evaluated through universal testing device (STM 20, SANTAM Ltd, Iran) equipped with a 100 N load cell at the cross head speed of 1 mm/min. The following equations were used for calculating Young's modulus (E) (1) and ultimate compressive stress (σ) (2):

$$E = \frac{KL}{A} \quad (1)$$

$$\sigma = \frac{F}{A} \quad (2)$$

where K is the stiffness, L the length of sample, F the ultimate load, and A the average of surface area obtained from Eq. (3):

$$A = \frac{\pi}{2} \times \frac{1}{4} \times (d_1^2 - d_2^2) \quad (3)$$

where d_1 and d_2 are the diameters of the cylindrical specimens. The slope of the stress–strain curve at the fracture point is the value of K. The test was repeated three times for each sample.

2.7. Evaluation of in Vitro Acellular Behavior

The in vitro surface activity of the scaffolds was evaluated after soaking them in Simulated Body Fluid (SBF) at the solid-to-liquid ratio (S/L) of 1 g/100 mL and then, they were kept at 37 °C for several periods up to 28 days. The SBF solution was prepared based on the procedure suggested by Kokubo et al. [16] by dissolving NaCl 8.035 g/L, KCl 0.225 g/L, $K_2HPO_4.3H_2O$ 0.231 g/L, $MgCl_2.6H_2O$ 0.311 g/L, $CaCl_2$ 0.292 g/L, $NaHCO_3$ 0.355 g/L, and Na_2SO_3 0.072 g/L into distilled water, buffered at pH=7.25 with 6.118 g/L tris-hydroxymethyl aminomethane and 1 N HCl solution at 37 °C. The SBF solution was selected due to its highly supersaturated characteristic in terms of apatite. According to Oyane and Takadama [17,18], SBF is the best solution to evaluating the apatite-formation ability in biomaterials. The microstructure and surface morphology of the samples were observed using SEM after soaking them in the SBF solution for 14 and 28 days.

2.8. Procedure of Cell Culture and MTT Assay

Osteoblast-like cells of human (SaOS-2) were cultured in Dulbecco Modified Eagle Medium (DMEM;Gibco-BRL, LifeTech-nologies, GrandIsland, NY) supplemented with 15 % fetal bovine serum (FBS) (Dainippon Pharmaceutical, Osaka, Japan) in a 5 % CO_2 atmosphere at 37 °C. The scaffolds (with dimentions of $0.5\times0.5\times0.5$ cm^3 were sterilized using 70 % ethanol, and the cells were seeded over them at 2×10^4 cells/well [19]. Similarly, discs with similar dimensions were prepared from the culture dish (polystyrene) and used as the control group. The sample/cell constructs were placed into 24-well culture plates and left in an incubator for three hours to allow cell attachment. Next, 3 mL of culture medium was added into each well, and the cell/specimen constructs were cultured in a humidified incubator at 37 °C with 95 % air and 5 % CO_2 for 2 and 7 days. The medium was changed every 3 days.

SEM was employed to monitor the morphology of the attached cells. For this purpose, followed by cell fixation, the specimens were dehydrated in ethanol solutions for about 20 min. They were then dried in the air, coated with gold, and analyzed by SEM.

The cell proliferation in contact with the samples was measured by using water soluble enzyme substrate 3-(4,5-dimethylthiazol-2-yl)-2,5-diphenyl tetrazolium bromide (MTT, Sigma, Germany), which turned into a purple water insoluble product formazan accumulated in

the cytoplasm of viable cells. In this regard, at the end of each period, the medium was removed, and 2 mL of MTT solution was added to each well. Followed by incubation at 37 °C for four hours in a fully humidified atmosphere (5 % CO_2/95 % air), MTT was taken up by active cells and reduced to insoluble purple formazan granules in mitochondria. Subsequently, the medium was thrown away, the precipitated formazan was dissolved in dimethyl sulfoxide (DMSO, Sigma, Germany) (150 mL/well), and the optical density of the solution was measured using a microplate spectrophotometer (BIO-TEK Elx 800, Highland park, USA) at 570 nm. Cell number was determined using a linear correlation between the absorbance and cell concentration.

2.9. Statistical Analysis

Data were calculated by Microsoft Excel 2019 software, the results of which were reported as the mean ± standard deviation of at least three experiments. The significance among the mean values was determined using standard software program (SPSS GmbH, Munich, Germany) such that the probability values less than 0.05 ($P \leq 0.05$) were considered significant.

3. RESULTS AND DISCUSSION

The DTA and TG analyses of the BG were carried out to acquire the exact sintering temperature, as shown in Figure 1. The first endothermic peak initiated at 120 °C corresponds to the release of physically adsorbed water. According to the TGA diagram, it was removed between 50 °C and 150 °C (No. 1). There is an exothermic peak at 320 ºC which can be attributed to the release of structural water that leads to weight loss between 150 °C and 400 °C (No. 2). Two other endothermic peaks (No. 3 and 4), started at 550 °C, are associated with the removal of silanol and nitrate groups that are usually eliminated in the thermal stabilization process [20]. Approximately 10 % of the total weight loss occurred by removal of all nitrates at 600 °C. Finally, the crystallization process of $CaSiO_3$ (β-wollastonite) and cristobalite (SiO_2) was completed around 970 °C (No. 6) [20], which was found to occur at higher temperatures in similar glasses [21,22].

Negligible weight loss was observed above 700 °C, indicating that the residuals were removed before 700 °C [4], hence this temperature was found to be propper for stabilization of the glass structure. Of note, the glass transition temperature of the dried gel occured at about 800 °C (No. 5). Controlling the sintering temperature is a fundamental factor that affects apatite formation. As reported, the heat treatment of the bioglass as a coating affected bioactivity. According to the studies, an imperfect apatite layer was formed on the bioglass. In fact, crystallisation decreased the bioactivity of the bioglass that was coated on the porous alumina scaffold and prepared by slip casting [23].

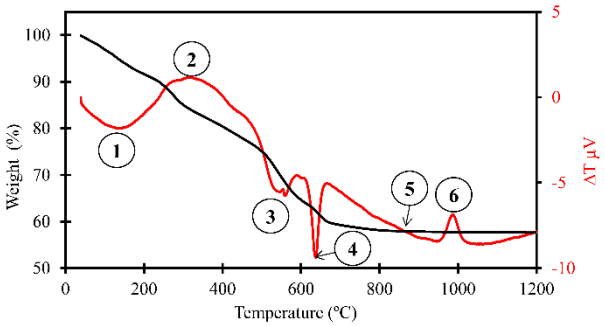

Figure 1. DTA (red line) and TG (black line) analyses of the BG

Figure 2 illustrates the XRD patterns of the sintered alumina at 1700 °C, stabilized BG at 800 °C, and coated scaffold. No diffraction peak was observed in the XRD pattern of BG, and the sample was almost amorphous due to its internal disorder. In this respect, 800 °C was selected as the suitable temperature for BG stabilization. According to the pattern of the coated alumina scaffold, the corundum phase (JCPDS Card No 46-1212) at pure alumina scaffold was converted to sillimanite (a composition of Al_2O_3-SiO_2) with JCPDS Card No 22-0018 partially followed by sitering at 800 °C, indicating that the silica in the structure of BG was diffused in alumina scaffold, hence formation of the sillimanite phase.

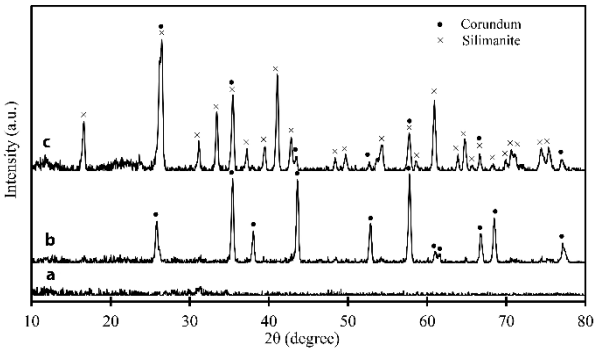

Figure 2. X-Ray diffraction patterns of a) BG stabilized at 800 °C, b) Sintered alumina at 1650 °C, and c) BG coated Al-scaffold

Figure 3 shows the micrograph of the sintered scaffolds prepared by different polyurethane foams. As expected, all prepared scaffolds thorugh replica method were highly porous so that the size of pores and their walls increased by decreasing PPI. The mean size of the pores and their walls were estimated using Image J software and SEM images. The given data in Table 1 show that the average pore size of the scaffold prepared by 30 PPI foam is 1133 µm which decrease to 376 µm in the sample prepared by 60 PPI foam. The results of the calculated porosity percentage from Equation 1 are also given in

Table 1. The prepared sample with 60 PPI foam had the highest porosity percentage. On the contrary, the porous alumina-based ceramics fabricated by Polymethylmethacrylate (PMMA) microspheres had the mean pore size of about 22.6 µm and open porosity percentage of 62 %. In other words, they had smaller pore size and less porosity percentage than those of the scaffolds prepared by foam replica, hence higher mechanical strength can be expected [24].

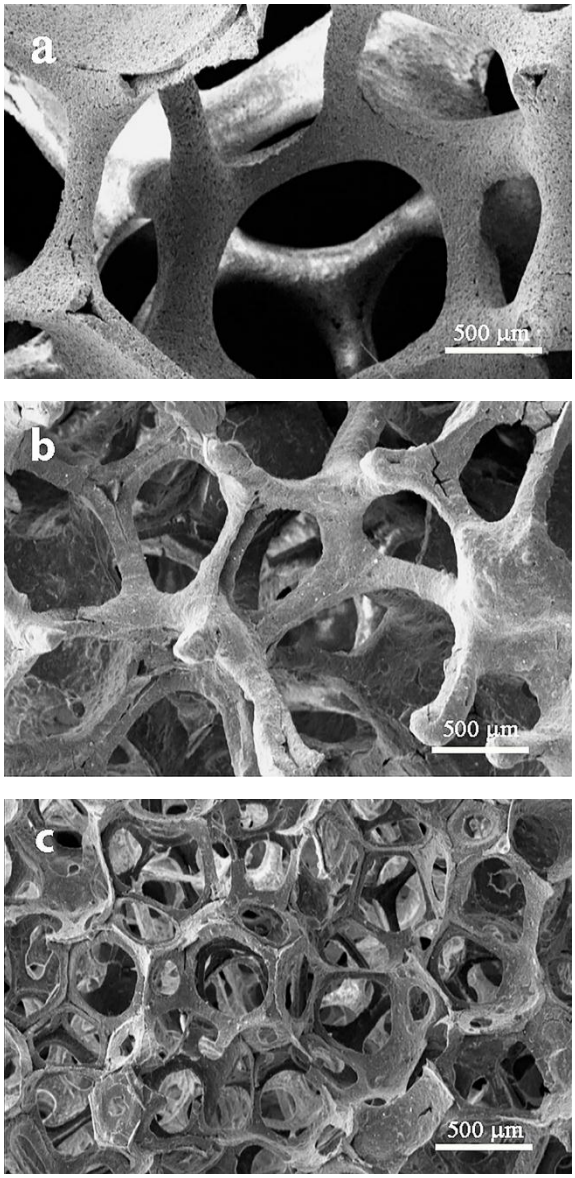

Figure 3. SEM images of scaffolds prepared by a) 30 PPI, b) 45 PPI, and c) 60 PPI polyurethane foams

Table 1 presents the results of the mechanical strength of the scaffolds. According to this table, the compressive strength decreased upon increasing the porosity percentage of the scaffolds. The compressive strength of the scaffold prepared by 30 PPI foam was 1.75 MPa which was higher than that of the other samples. The compressive strength of the trabecular bone was between 0.22 MPa and 10.44 MPa, and the mean value was about 3.9 MPa [25-28]. Therefore, this scaffold can be recommended to be used for tissue repair of the trabecular bone. In addition, the porosity diameter of the scaffold prepared through template replica method was considerably high, hence useful for TE applications [22]. Moreover, the scaffold possesses interconnected porosities. Pore connectivity plays an important role in the penetration into the scaffold [29].

TABLE 1. The Characteristics of porosity and mechanical properties of prepared scaffolds with different polyurethane foams

Types of polyurethane foams	**30 PPI**	**45 PPI**	**60 PPI**
Diameter of Pore (µm)	1133±50	550±24	376±13
Diameter of pore's wall (µm)	275±24	185±18	79±11
Calculated porosity (%)	79.5±0.5	85.05±0.03	93.41±0.65
Compressive strength (MPa)	1.75±0.5	0.51±0.2	0.35±0.1

Therefore, the synthesized sample through foam PPI No.: 30 can be regarded as the Optimum Alumina Scaffold (OAS). The composition of OAS is exactly the same as that of other samples (BG coated alumina); they only differ in the applied foam.

To measure the thickness of BG coating, SEM observation at different magnifications was used. As observed in Figure 4, the coating thickness is nearly 1.5 µm, and it is tightly attached to the alumina scaffold. To obtain an strong coating, the thermal expansion coefficients of both substrate and coating layer must be matched. Otherwise, the created thermal stresses between the substrate and coating would cause cracks. In this study, the thermal expansion coefficient of BG was measured based the rule of mixtures as 4.92×10^{-6} °C^{-1}. The thermal expansion coefficient of alumina was also 9.47×10^{-6} °C^{-1}. Due to the smaller coefficient value of the BG, the stresses in the coating would be compressive, thus forming a good bonding between the BG and alumina substrate. Figure 4 presents the EDS analysis of the substrate and coating of OAS. All of the constituent elements of the BG were identifiable in the the coating layer. The elements of Al and Si were also found in the substrate. The presence of Si in the substrate confirmed that the sol was infiltrated into the scaffold structure which in turn led to the formation of a new phase of Al_2O_3-SiO_2 in accordance with the XRD results.

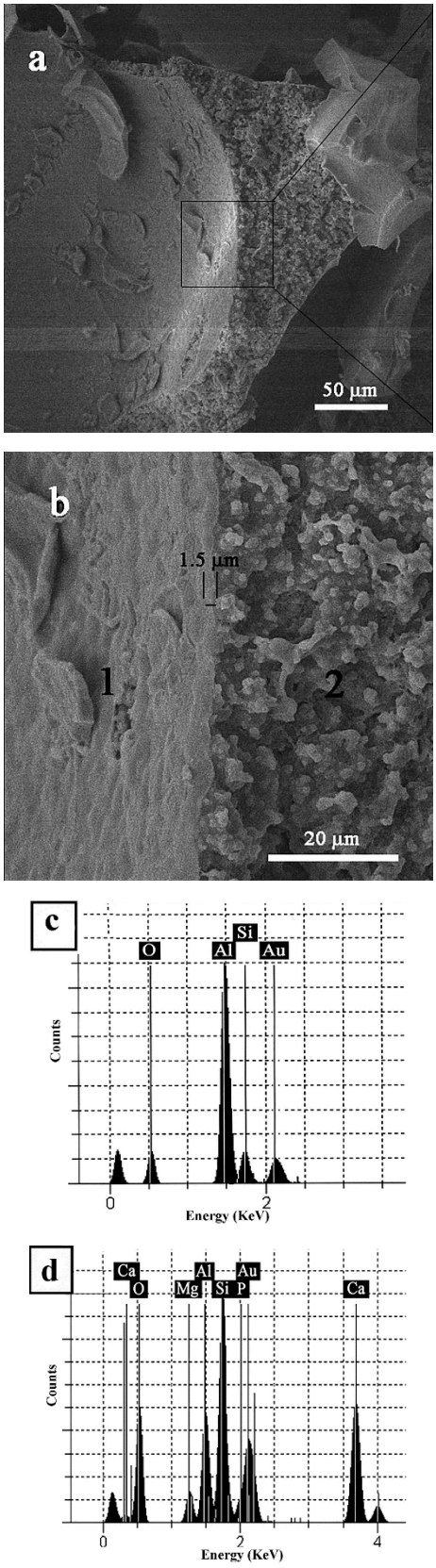

Figure 4. SEM of the BG coated alumina scaffold at different magnifications a) 400 X, b) 2000 X, and EDS analysis of c) the coating (point 1) and d) the substrate (point 2) of the scaffold

Figure 5 illustrates the BG-coated OASs after 14 and 28 days of immersion in SBF solution. As seen, the hydroxyapatite layer with a spherical morphology was precipitated after 14 days. Obviously, a ball-like morphology containing the entangled crystals was observed on the surface of the sample after 28 days. This kind of apatite morphology is fromed through the dissolution-precipitation mechanism. According to other researches [30], changes in the surface chemistry and topography in vitro were controlled by the solubility of the different phases. The reaction between the phosphate ions of SBF and released calcium ions by the material cause the nucleation of a calcium-deficient hydroxyapatite layer. These surfaces were formed after 28 days due to the abovementioned mechanism [31]. The elemental image analyses of the surface are illiustrated in the corner of Figure 5. The presence of Ca and P peaks determines the formation of a calcium phosphate layer.

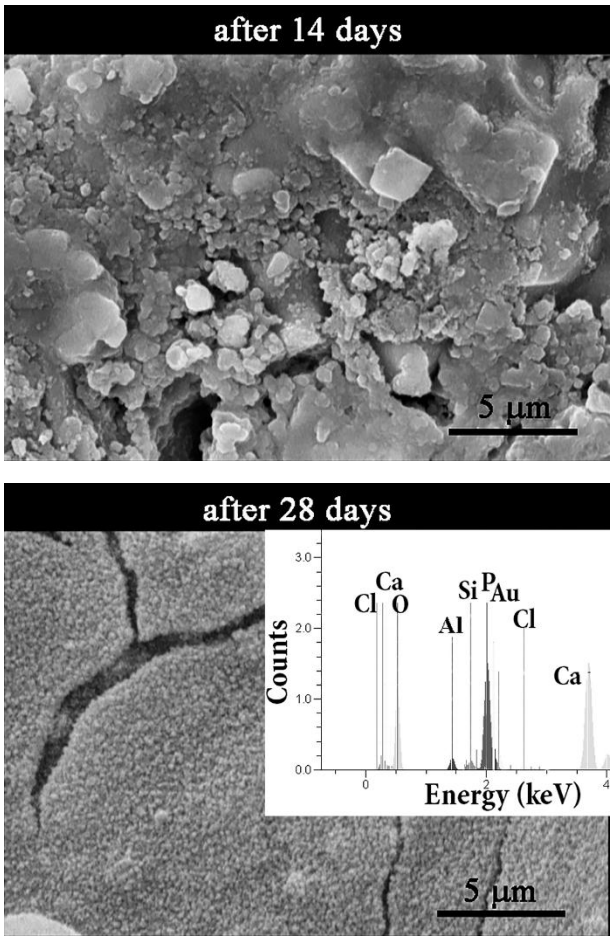

Figure 5. SEM observation of the BG coated alumina scaffold after 14 and 28 days of soaking in SBF solution. (in the corner: EDS analysis of the surface)

Figure 6 shows the SEM micrographs of alumina scaffolds and BG-coated OASs after 2 and 7 days of

osteoblastic cell culture in different magnifications. SEM is a beneficial method to detecting the morphology and distribution of cells on the surface of scaffolds [32]. According to this figure, Alumina did not adversely affect cell proliferation, and cells were properly attached and spread on the surface due to the compatibility and proper topography of the samples in terms of cell growth. The cells are marked with white arrows in Figure 6.

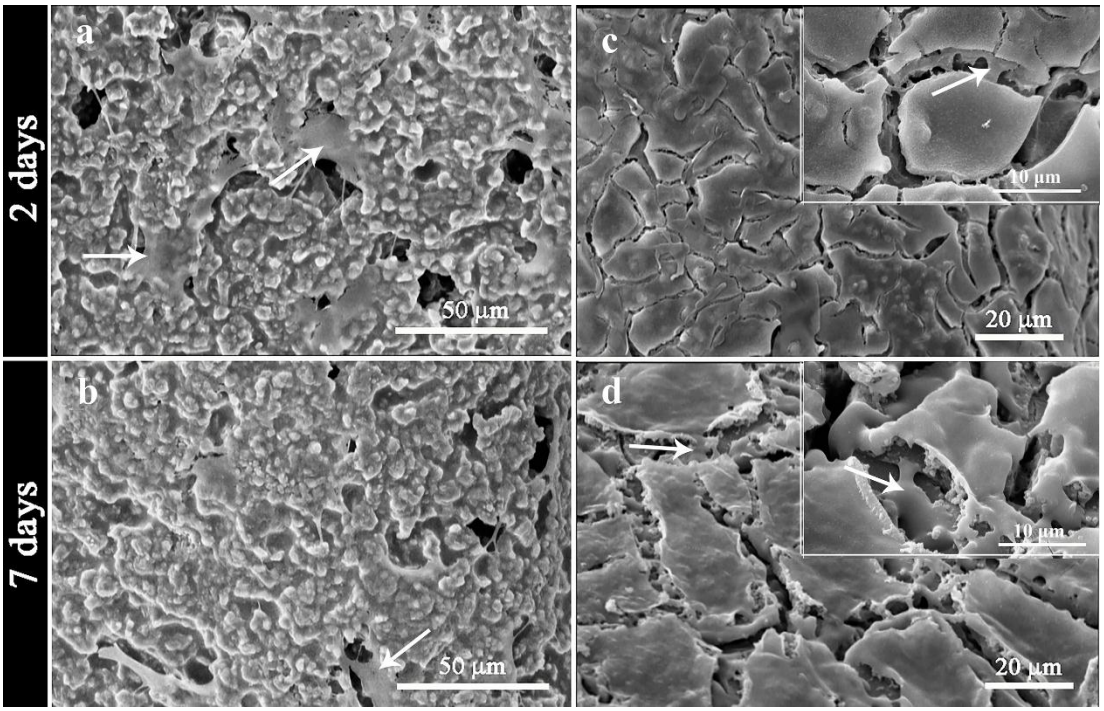

Figure 6. SEM micrographs of alumina scaffolds a) after 2 days, b) after 7 days, BG coated alumina scaffolds c) after 2 days and d) after 7 days of osteoblastic cell culture (at the corner of image, higher magnification is observed where white arrows indicate spread cells)

The obtained results were in good agreement with those from another research carried out by Bose and et al. [33]. Apparantly, after 7 days, the cells covered a larger area of the scaffold surface. In case the matrix is inappropriate or toxic, the cells would be less extended over the surface [34].

The cytotoxicity study on the specimens was conducted using the MTT colorimetric method to confirm the microscopic observations. Figure 7 shows the proliferation of the osteoblasts on different specimens. The results of the studies at 2 and 7 days revealed that the number of cells on the surfaces of aluminum and BG- coated aluminum scaffolds increased significantly with time. The differences in the cell numbers between days 2 and 7 are statistically significant ($P \leq 0.05$); therefore, after cell attachment, proliferation begins on all samples. On days 2 and 7, the numbers of cells proliferated on aluminum and BG-coated aluminum scaffolds were compared, and it was found that the differences between the average values were not statistically important. However, the number of cells on polystyrene was extremely lower than that of aluminum and BG-coated aluminum scaffolds with no cytotoxicity of the samples.

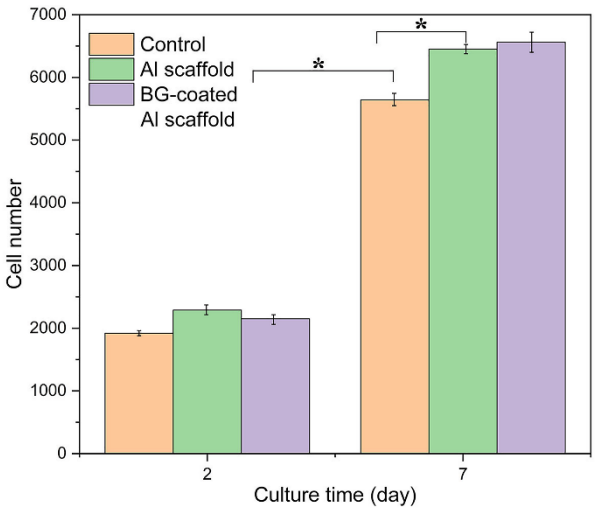

Figure 7. Proliferation of osteoblasts on Al scaffold, BG-coated Al scaffold, and control sample measured by MTT assay (*$P \leq 0.05$)

The scaffold material provides a substrate for cell attachment, proliferation, and differentiation [35]. In order to obtain a scaffold for bone regeneration in this study, both alumina and BG-coated based scaffolds were prepared. The surface topography of the biomaterial affected cellular responses in vitro preferably, hence bioactive materials should interact with cells to motivate cell ingrowth [36]. Cell attachment is the primary stage of the interaction between the cells and biomaterial [37]. The surface of the biomaterials affects the morphology of cells that define biocompatibility [38]. The SEM results of cell morphology revealed that cell cover on the surface of COAS was better than that of OAS. In other words, cellular responses to biomaterials depends not only on the surface morphology but on the chemical composition of the biomaterial [39], which plays a fundamental role in determining interaction between the cells and materials by changing the quantity of the released ions from the biomaterial [40]. In this study, a sol–gel derived bioactive glasses containing SiO_2, CaO, and P_2O_5 was selected as the coating. SiO_2 is a network former in the glass structure. Moreover, Si–OH groups produced from the exchange process of Ca^{2+} ions (from glass) with H_3O^+ (from solution) are susceptible sites for calcium phosphate nucleation [41,42]. At the same time, Si ions released from the glass composition into the medium can accelerate cell functions [43,44]. P_2O_5 is also used to encourage nucleation of calcium phosphate phase on the glass surfaces [45].

4. CONCLUSIONS

The following conclusions can be derived from this study:

- Alumina was transformed to sillimanite phase when coating the alumina scaffold with BG as a result of the diffusion of silicon into the scaffold as well as the reaction of alumina with silicon.
- The mechanical strength decreased upon increasing the porosity percentage of the scaffolds.
- According to the SEM observation, the spherical hydroxyapatite particles were formed well on the surface of BG-coated alumina scaffold after different time intervals of being soaked in SBF solution.
- According to the preliminary in vitro test data, both alumina and BG-coated scaffolds were not toxic after processing, and they provided favorite sites for cell attachment and proliferation for SaOS-2 cells.
- The bioactivity properties of the BG-coated alumina scaffold were significant since they exhibited acceptable cell attachment and cell growth. The results of experiments confirmed the application of the prepared scaffold in bone regeneration field.

ACKNOWLEDGEMENTS

The authors wish to acknowledge Imam Khomeini International University-Buin Zahra Higher Education Center of Engineering and Technology and Materials and Energy Research Center (MERC) for the all supports.

REFERENCES

1. Ramay, H. R., Zhang, M., "Biphasic calcium phosphate nanocomposite porous scaffolds for load-bearing bone tissue engineering", ***Biomaterials***, Vol. 25, No. 21, (2004), 5171-5180. https://doi.org/10.1016/j.biomaterials.2003.12.023
2. Zhu, G., Zhang, T., Chen, M., Yao, K., Huang, X., Zhang, B., Li, Y., Liu, J., Wang, Y., Zhao, Z., "Bone physiological microenvironment and healing mechanism: basis for future bone-tissue engineering scaffolds", ***Bioactive Materials***, Vol. 6, No. 11, (2021), 4110-4140. https://doi.org/10.1016/j.bioactmat.2021.03.043
3. Alonzo, M., Primo, F. A., Kumar, S. A., Mudloff, J. A., Dominguez, E., Fregoso, G., Ortiz, N., Weiss, W. M., Joddar, B., "Bone tissue engineering techniques, advances, and scaffolds for treatment of bone defects", ***Current Opinion in Biomedical Engineering***, Vol. 17, (2021), 100248. https://doi.org/10.1016/j.cobme.2020.100248
4. Tsang, V. L., Bhatia, S. N., "Three-dimensional tissue fabrication", ***Advanced Drug Delivery Reviews***, Vol. 56, No. 11, (2004), 1635-1647. https://doi.org/10.1016/j.addr.2004.05.001
5. Bohner, M., Van Lenthe, G. H., Grünenfelder, S., Hirsiger, W., Evison, R., Müller, R., "Synthesis and characterization of porous β-Tricalcium phosphate blocks", ***Biomaterials***, Vol. 26, No. 31, (2005), 6099-6105. https://doi.org/10.1016/j.biomaterials.2005.03.026
6. Zhang, J., Wu, L., Jing, D., Ding, J., "A comparative study of porous scaffolds with cubic and spherical macropores", ***Polymer***, Vol. 46, No. 13, (2005), 4979-4985. https://doi.org/10.1016/j.polymer.2005.02.120
7. Sokolsky-Papkov, M., Agashi, K., Olaye, A., Shakesheff, K., Domb, A. J., "Polymer carriers for drug delivery in tissue engineering", ***Advanced Drug Delivery Reviews***, Vol. 59, No. 4-5, (2007), 187-206. https://doi.org/10.1016/j.addr.2007.04.001
8. Kim, Y. H., Anirban, J. M., Song, H. Y., Seo, H. S., Lee, B. T., "In vitro and In vivo evaluations of 3D porous TCP-coated and non-coated alumina scaffolds", ***Journal of Biomaterials Applications***, Vol. 25, No. 6, (2011), 539-558. https://doi.org/10.1177/0885328209356945
9. Naga, S. M., Awaad, M., El-Maghraby, H. F., El-Kady, A. M., "Biological performance of calcium pyrophosphate-coated porous alumina scaffolds", ***International Journal of Applied Ceramic Technology***, Vol. 11, No. 1, (2014), 1-11. https://doi.org/10.1111/ijac.12076
10. Camilo, C. C., Fortulan, C. A., Ikegami, R. A., Santos, A. R., Purquerio, B. de M., "Manufacturing of porous alumina scaffolds with bio-glass and HAp coating: Mechanical and In vitro evaluation", In Prado M., Zavaglia, C. (eds.), ***Key Engineering Materials***, Trans Tech Publications Ltd., Switzerland, Vol. 396-398, (2009), 679-682. https://doi.org/10.4028/www.scientific.net/KEM.396-398.679
11. Jun, Y. K., Kim, W. H., W., Kweon, O. K., Hong, S. H., "The fabrication and biochemical evaluation of alumina reinforced calcium phosphate porous implants", ***Biomaterials***, Vol. 24, No. 21, (2003), 3731-3739. https://doi.org/10.1016/S0142-9612(03)00248-5
12. González, P., Serra, J., Liste, S., Chiussi, S., León, B., Pérez-Amor, M., Martínez-Fernández, J., de Arellano-López, A. R., Varela-Feria, F. M., "New biomorphic SiC ceramics coated with bioactive glass for biomedical applications", ***Biomaterials***, Vol.

24, No. 24, (2003), 4827-4832. https://doi.org/10.1016/S0142-9612(03)00405-8
13. Tonda-Turo, C., Gentile, P., Saracino, S., Chiono, V., Nandagiri, V. K., Muzio, G., Canuto, R. A., Ciardelli, G., "Comparative analysis of gelatin scaffolds crosslinked by genipin and silane coupling agent", ***International Journal of Biological Macromolecules***, Vol. 49, No. 4, (2011), 700-706. https://doi.org/10.1016/j.ijbiomac.2011.07.002
14. Nadeem, D., Kiamehr, M., Yang, X., Su, B., "Fabrication and in vitro evaluation of a spongelike bioactive-glass/gelatin composite scaffold for bone tissue engineering", ***Material Science and Engineering: C***, Vol. 33, No. 5, (2013), 2669-2678. https://doi.org/10.1016/j.msec.2013.02.021
15. Barabadi, Z., Azami, M., Sharifi, E., Karimi, R., Lotfibakhshaiesh, N., Roozafzoon, R., Joghataei, M. T., Ai, J., "Fabrication of hydrogel based nanocomposite scaffold containing bioactive glass nanoparticles for myocardial tissue engineering", ***Materials Science and Engineering: C***, Vol. 69, (2016), 1137-1146. https://doi.org/10.1016/j.msec.2016.08.012
16. Kokubo, T., Kushitani, H., Sakka, S., Kitsugi, T., Yamamuro, T., "Solutions able to reproduce In vivo surface-structure changes in bioactive glass-ceramic A-W^{3}", ***Journal of Biomedical Material Research***, Vol. 24, No. 6, (1990), 721-734. https://doi.org/10.1002/jbm.820240607
17. Oyane, A., Kim, H. M., Furuya, T., Kokubo, T., Miyazaki, T., Nakamura, T., "Preparation and assessment of revised simulated body fluid", ***Journal of Biomedical Materials Research Part A: An Official Journal of The Society for Biomaterials, The Japanese Society for Biomaterials, and The Australian Society for Biomaterials and the Korean Society for Biomaterials***, Vol. 65, No. 2, (2003), 188-195. https://doi.org/10.1002/jbm.a.10482
18. Takadama, H., Hashimoto, M., Mizuno, M., Kokubo, T., "Round-robin test of SBF for In vitro measurement of apatite-forming ability of synthetic materials", ***Phosphorus Research Bulletin***, Vol. 17, (2004), 119-125. https://doi.org/10.3363/prb1992.17.0_119
19. Khorami, M., Hesaraki, S., Behnamghader, A., Nazarian, H., Shahrabi, S., "In vitro bioactivity and biocompatibility of lithium substituted 45S5 bioglass", ***Material Science and Engineering: C***, Vol. 31, No. 7, (2011), 1584-1592. https://doi.org/10.1016/j.msec.2011.07.011
20. Saravanapavan, P., Jones, J. R., Pryce, R. S., Hench, L. L., "Bioactivity of gel-glass powders in the CaO-SiO_2 system: A comparison with ternary (CaO-P_2O_5-SiO_2) and quaternary glasses (SiO_2-CaO-P_2O_5-Na_2O)", ***Journal of Biomedical Materials Research Part A: An Official Journal of The Society for Biomaterials, The Japanese Society for Biomaterials, and The Australian Society for Biomaterials and the Korean Society for Biomaterials***, Vol. 66, No. 1, (2003), 110-119. https://doi.org/10.1002/jbm.a.10532
21. Jones, J. R., Ehrenfried, L. M., Hench, L. L., "Optimising bioactive glass scaffolds for bone tissue engineering", ***Biomaterials***, Vol. 27, No. 7, (2006), 964-973. https://doi.org/10.1016/j.biomaterials.2005.07.017
22. Greenspan, D. C., Zhong, J. P., LaTorre, G. P., "Effect of surface area to volume ratio on in vitro surface reactions of bioactive glass particulates", In Andersson, O. H., Happonen, R. P., Yli-Urpo, A. (eds.), Proceedings of the 7th International Symposium on Ceramics in Medicine, ***Bioceramics***, Oxford, London: Butterworth-Heinemann, Vol. 7, (1994), 55-60. https://doi.org/10.1016/B978-0-08-042144-5.50012-1
23. Komlev, V. S., Barinov, S. M., "Porous hydroxyapatite ceramics of bimodal pore size distribution", ***Journal of Materials Science: Materials in Medicine***, Vol. 13, No. 3, (2002), 295-299. https://doi.org/10.1023/A:1014015002331
24. Kamitani, K., Hyodo, T., Shimizu, Y., Egashira, M., "Fabrication of highly porous alumina-based ceramics with connected spaces by employing PMMA microspheres as a template", ***Advanced in Materials Science Engineering***, Vol. 2009, (2009), 601850. https://doi.org/10.1155/2009/601850
25. Misch, C. E., Qu, Z., Bidez, M. W., "Mechanical Properties of Trabecular Bone in the Human Mandible: Implications for Dental Implant Treatment Planning and Surgical Placement", ***Journal of Oral and Maxillofacial Surgery***, Vol. 57, No. 6, (1999), 700-706. https://doi.org/10.1016/S0278-2391(99)90437-8
26. Baptista, R., Guedes, M., "Morphological and mechanical characterization of 3D printed PLA scaffolds with controlled porosity for trabecular bone tissue replacement", ***Materials Science and Engineering: C***, Vol. 118 , (2021), 111528. https://doi.org/10.1016/j.msec.2020.111528
27. Burgers, T. A., Mason, J., Niebur, G., Ploeg, H. L., "Compressive properties of trabecular bone in the distal femur", ***Journal of Biomechanics***, Vol. 41, No. 5, (2008), 1077-1085. https://doi.org/10.1016/j.jbiomech.2007.11.018
28. Wu, D., Spanou, A., Diez-Escudero, A., Persson, C., "3D-printed PLA/HA composite structures as synthetic trabecular bone: A feasibility study using fused deposition modeling", ***Journal of the Mechanical Behavior of Biomedical Materials***, Vol. 103, (2020), 103608. https://doi.org/10.1016/j.jmbbm.2019.103608
29. Karageorgiou, V., Kaplan, D., "Porosity of 3D biomaterial scaffolds and osteogenesis", ***Biomaterials***, Vol. 26, No. 27, (2005), 5474-5491. https://doi.org/10.1016/j.biomaterials.2005.02.002
30. Sainz, M. A., Pena, P., Serena, S., Caballero, A., "Influence of design on bioactivity of novel $CaSiO_3$-$CaMg(SiO_3)_2$ bioceramics: In vitro simulated body fluid test and thermodynamic simulation", ***Acta Biomaterialia***, Vol. 6, No. 7, (2010), 2797-2807. https://doi.org/10.1016/j.actbio.2010.01.003
31. Rhee, S. H., "Effect of calcium salt content in the poly(E-caprolactone)/silica nanocomposite on the nucleation and growth behavior of apatite layer", ***Journal of Biomedical Materials Research Part A: An Official Journal of The Society for Biomaterials, The Japanese Society for Biomaterials, and The Australian Society for Biomaterials and the Korean Society for Biomaterials***, Vol. 67, No. 4, (2003), 1131-1138. https://doi.org/10.1002/jbm.a.20054
32. Teixeira, S., Ferraz, M. P., Monteiro, F. J., "Biocompatibility of highly macroporous ceramic scaffolds: cell adhesion and morphology studies", ***Journal of Materials Science: Materials in Medicine***, Vol. 19, No. 2, (2008), 855-859. https://doi.org/10.1007/s10856-007-3005-x
33. Bose, S., Darsell, J., Hosick, H. L., Yang, L., Sarkar, D. K., Bandyopadhyay, A., "Processing and characterization of porous alumina scaffolds", ***Journal of Materials Science: Materials in Medicine***, Vol. 13, No. 1, (2002), 23-28. https://doi.org/10.1023/A:1013622216071
34. Gutiérrez-Prieto, S. J., Perdomo-Lara, S. J., Diaz-Peraza, J. M., Sequeda-Castañeda, L. G., "Analysis of in vitro osteoblast culture on scaffolds for future bone regeneration purposes in dentistry", ***Advances in Pharmacological Sciences***, Vol. 2019, (2019), 5420752. https://doi.org/10.1155/2019/5420752
35. Reddi, A. H., "Symbiosis of Biotechnology and Biomaterials: Applications in Tissue Engineering of Bone and Cartilage", ***Journal of Cellular Biochemistry***, Vol. 56, No. 2, (1994), 192-195. https://doi.org/10.1002/jcb.240560213
36. Chen, Q. Z., Efthymiou, A., Salih, V., Boccaccini, A. R. "Biogalss®-derived glass-ceramic scaffolds: study of cell proliferation and scaffold degradation in vitro", ***Journal of Biomedical Materials Research Part A: An Official Journal of The Society for Biomaterials, The Japanese Society for Biomaterials, and The Australian Society for Biomaterials and the Korean Society for Biomaterials***, Vol. 84, No. 4, (2008), 1049-1060. https://doi.org/10.1002/jbm.a.31512
37. Low, S. P., Williams, K. A., Canham, L. T., Voelcker, N. H., "Evaluation of mammalian cell adhesion on surface modified porous silicon", ***Biomaterials***, Vol. 27, No. 26, (2006), 4538-4546. https://doi.org/10.1016/j.biomaterials.2006.04.015
38. Lee, J., Kang, B. S., Hicks, B., Chancellor Jr., T. F., Chu, B. H., Wang, H. T., "The control of cell adhesion and viability by zinc oxide nanorods", ***Biomaterials***, Vol. 29, No. 27, (2008), 3743-3749. https://doi.org/10.1016/j.biomaterials.2008.05.029

39. Chou, S. Y., Cheng, C. M., LeDuc, P. R., "Composite polymer systems with control of local substrate elasticity and their effect on cytoskeletal and morphological characteristics of adherent cells", ***Biomaterials***, Vol. 30, No. 18, (2009), 3136-3142. https://doi.org/10.1016/j.biomaterials.2009.02.037
40. Wu, C., Ramaswmy, Y., Zhu, Y. F., Zheng, R., Appleyard, R., Howard, A., Zreiqat, H., "The effect of mesoporous bioactive glass on the physiochemical, biological and drug-release properties of poly (DL-lactide-co-glycolide) films", ***Biomaterials***, Vol. 30, No. 12, (2009), 2199-2208. https://doi.org/10.1016/j.biomaterials.2009.01.029
41. Seeman, E., Devogelaer, J. P., Lorenc, R., Spector, T., Brixen, K., Balogh, A., Stucki, G., Reginster, J. Y., "Strontium ranelate reduces the risk of vertebral fractures in patients with osteopenia", ***Journal of Bone and Mineral Research***, Vol. 23, No. 3, (2008), 433-438. https://doi.org/10.1359/jbmr.071105
42. Panzavolta, S., Torricelli, P., Sturba, L., Bracci, B., Giardino, R., Bigi, A., "Setting properties and in vitro bioactivity of strontium-enriched gelatin-calcium phosphate bone cements", ***Journal of Biomedical Materials Research Part A: An Official Journal of The Society for Biomaterials, The Japanese Society for Biomaterials, and The Australian Society for Biomaterials and the Korean Society for Biomaterials***, Vol. 84, No. 4, (2008), 965-972. https://doi.org/10.1002/jbm.a.31412
43. Pietak, A. M., Reid, J. W., Stott, M. J., Sayer, M., "Silicon substitution in the calcium phosphate bioceramics", ***Biomaterials***, Vol. 28, No. 28, (2007), 4023-4032. https://doi.org/10.1016/j.biomaterials.2007.05.003
44. Phan, P. V., Grzanna, M., Chu, J., Polotsky, A., El-Ghannam, A., Van Heerden, D., Hungerford, D. S., Frondoza, C. G., "The effect of silica-containing calcium-phosphate particles on human osteoblasts In vitro", ***Journal of Biomedical Materials Research Part A: An Official Journal of The Society for Biomaterials, The Japanese Society for Biomaterials, and The Australian Society for Biomaterials and the Korean Society for Biomaterials***, Vol. 67, No. 3, (2003), 1001-1008. https://doi.org/10.1002/jbm.a.10162
45. Buehler, J., Chappuis, P., Saffar, J. L., Tsouderos, Y., Vignery, A., "Strontium ranelate inhibits bone resorption while maintaining bone formation in alveolar bone in monkeys (Macaca fascicularis)", ***Bone***, Vol. 29, No. 2, (2001), 176-179. https://doi.org/10.1016/S8756-3282(01)00484-7